JACS
JOURNAL OF THE AMERICAN CHEMICAL SOCIETY

Article

pubs.acs.org/JACS

$[Cu_2O]^{2+}$ Active Site Formation in Cu−ZSM-5: Geometric and Electronic Structure Requirements for N_2O Activation

Ming-Li Tsai,[†] Ryan G. Hadt,[†] Pieter Vanelderen,[‡] Bert F. Sels,*[,‡] Robert A. Schoonheydt,*[,‡] and Edward I. Solomon*[,†]

[†]Department of Chemistry, Stanford University, Stanford, California 94305, United States

[‡]Center for Surface Chemistry and Catalysis, K. U. Leuven, Kasteelpark Arenberg 23, B-3001 Leuven, Belgium

Supporting Information

ABSTRACT: Understanding the formation mechanism of the $[Cu_2O]^{2+}$ active site in Cu−ZSM-5 is important for the design of efficient catalysts to selectively convert methane to methanol and related value-added chemicals and for N_2O decomposition. Spectroscopically validated DFT calculations are used here to evaluate the thermodynamic and kinetic requirements for formation of $[Cu_2O]^{2+}$ active sites from the reaction between binuclear Cu^I sites and N_2O in the 10-membered rings Cu−ZSM-5. Thermodynamically, the most stable Cu^I center prefers bidentate coordination with a close to linear bite angle. This binuclear Cu^I site reacts with N_2O to generate the experimentally observed $[Cu_2O]^{2+}$ site. Kinetically, the reaction coordinate was evaluated for two representative binuclear Cu^I sites. When the Cu−Cu distance is sufficiently short (<4.2 Å), N_2O can bind in a "bridged" μ-1,1-O fashion and the oxo-transfer reaction is calculated to proceed with a low activation energy barrier (2 kcal/mol). This is in good agreement with the experimental E_a for N_2O activation (2.5 ± 0.5 kcal/mol). However, when the Cu−Cu distance is long (>5.0 Å), N_2O binds in a "terminal" η^1-O fashion to a single Cu^I site of the dimer and the resulting E_a for N_2O activation is significantly higher (16 kcal/mol). Therefore, bridging N_2O between two Cu^I centers is necessary for its efficient two-electron activation in $[Cu_2O]^{2+}$ active site formation. In nature, this N_2O reduction reaction is catalyzed by a tetranuclear Cu_Z cluster that has a higher E_a. The lower E_a for Cu−ZSM-5 is attributed to the larger thermodynamic driving force resulting from formation of strong Cu^{II}−oxo bonds in the ZSM-5 framework.

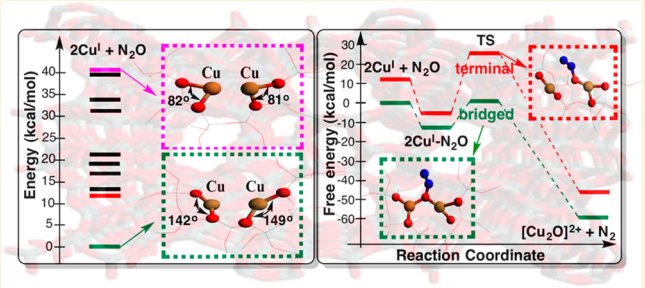

1. INTRODUCTION

Depletion of fossil fuel sources within the last few decades has significantly increased the demands for petroleum alternatives. Methane, the main component of abundant natural gas, has been recognized as a potential solution as it can be selectively oxidized to methanol, itself a viable fuel and an important precursor for chemical feedstocks and future fuel resources.[1,2] The current protocol for industrial methanol production involves the initial energy-consuming steam reformation of methane to syngas, a mixture of H_2 and CO, which is further reacted over a copper/zinc oxide/alumina-based catalyst at high temperatures and pressures to form CH_3OH.[3] In order to develop a more efficient means of converting methane to methanol, development of robust catalysts that are capable of selective oxidation of the strong C−H bond of methane (~104 kcal/mol) to methanol in a single step, under mild conditions, is imperative.[4,5] Recently, O_2- and N_2O-activated Cu−ZSM-5 have been demonstrated to convert methane to methanol with a low activation energy ($E_a \approx 15.7$ kcal/mol) and high selectivity (>98%) at relatively low temperature (~100 °C) and atmospheric pressure.[6,7] In addition to this unique reactivity in the methane to methanol conversion, the associated active site has also been demonstrated to have superior activity in the catalytic decomposition of chemically inert N_2O.[8−12]

Although initial studies attempted to characterize the nature of the reactive species in O_2- and N_2O-activated Cu−ZSM-5, no definitive conclusion was achieved due to the limitations of bulk spectroscopic methods (including extended X-ray absorption fine structure (EXAFS), absorption spectroscopy (abs), and electron paramagnetic resonance (EPR)) in distinguishing a small fraction of active species from the predominantly spectator copper background.[6,9] As the conversion of methane to methanol had been directly correlated to a characteristic 22 700 cm^{-1} absorption band,[8] resonance Raman (RR) spectroscopy using laser excitation into this electronic transition provided a site-selective probe. These vibrational data, including their oxygen isotope perturbations, allowed for identification of the reactive species in Cu−ZSM-5 as a bent $[Cu_2O]^{2+}$ core.[13,14]

Initial formation of Cu^I in the zeolite lattice by autoreduction is required for activation of O_2 and N_2O to form the $[Cu_2O]^{2+}$ core.[8,10,15] Spectroscopic (photoluminescence, IR, EXAFS),

Received: November 7, 2013
Published: February 13, 2014

   dx.doi.org/10.1021/ja4113808 | J. Am. Chem. Soc. 2014, 136, 3522−3529

structural (X-ray crystallography), and computational studies have been conducted to understand the Cu^I coordination environment in the ZSM-5 framework.[16−24] The $2Cu^I$ binding sites in the 10-membered ring of ZSM-5 have been generally described as bi- or tridentate with Cu^I bound to the lattice oxygens of two Al T sites separated by two Si T sites. However, the geometric and electronic requirements for the Cu^I−ZSM-5 sites to form the $[Cu_2O]^{2+}$ species have not been explored. Previous spectroscopic studies have shown that both O_2 and N_2O activation of autoreduced Cu−ZSM-5 generates the same $[Cu_2O]^{2+}$ site.[13] While formation from O_2 requires two additional electrons and loss of one oxo atom to the lattice, N_2O activation is more direct as it involves oxo transfer to two Cu^I centers (a two-electron process) with release of N_2.[13,25]

In this study, we focus on the mechanism of N_2O activation. DFT calculations verified through correlation to the spectral features of the $[Cu_2O]^{2+}$ core are used to identify an active binuclear Cu^I site (distinguished from a number of other potential binuclear and mononuclear Cu^I sites) in the 10-membered rings of Cu−ZSM-5. The activation barriers for a variety of N_2O binding modes on this binuclear Cu^I site and other nonreactive Cu^I sites are obtained from the potential energy surfaces (PESs) for N−O cleavage and correlated to the experimental E_a. This elucidates the thermodynamic and kinetic requirements for formation of the $[Cu_2O]^{2+}$ active site from N_2O. Interestingly, in the terminal step of bacterial denitrification, nature has employed a μ_4-sulfide-bridged tetranuclear copper cluster (i.e., the Cu_Z site) in the enzyme nitrous oxide reductase (N_2OR) to catalyze conversion of N_2O to N_2.[26−31] Comparison of Cu−ZSM-5 and N_2OR provides insights into the requirements for this conversion and general strategies for efficient N_2O activation.[32−38]

2. MATERIAL AND METHODS

Preparation of autoreduced Cu−ZSM-5 and its reaction with N_2O to generate the $[Cu_2O]^{2+}$ species were conducted based on previously published protocols.[10,15,39,40] More specifically, reactions of autoreduced Cu−ZSM-5 and N_2O were carried out in a fixed bed reactor setup under carefully chosen reaction conditions to avoid film and pore diffusion.[41] A 0.3 g amount of Cu−ZSM-5 catalyst (with an average catalyst particle size of 1 μm containing about 1.1×10^{-4} mmol of Cu of which about 5−10% is involved in formation of mono-μ-oxo dicopper) is loaded in a reactor (with a reactor volume, 1 cm^3). The catalyst was then exposed to a flow of pure oxygen (2 h at 723 K), followed by a He treatment overnight at 773 K. Subsequently, the reactor was cooled to the reaction temperature, ranging from 300 to 373 K, and contacted with a flow of N_2O in He (50 cm^3/min; 5 vol %). Computationally, the binding of Cu^I centers on lattice oxygens and the environment of the Al T sites in the ZSM-5 framework was modeled with SiH_3-capped lattice oxygens (86 atoms; the model in ref 13 had H caps and 68 atoms) (Figure S1A, Supporting Information) to avoid artificial Cu^I−OH interactions. This model was tested by addition of another lattice layer (140 atoms) with no significant change related to the 86-atom cluster presented below (see Figure S1C, Supporting Information). Two Si T sites separated by two Si T units within the 10-membered rings of ZSM-5 were replaced by Al T sites to construct 10 possible pairs of fully optimized $[Cu_2O]^{2+}$ sites. The presence of the Al provides the charge compensation for the Cu and stabilizes the binding of the Cu to the lattice by 20 kcal/mol. Their corresponding $2Cu^I$ sites were obtained by removing the bridging oxo and subsequent geometry optimization. Note that 10 of 12 T sites in the asymmetric unit of the MFI framework were replaced with Al T sites to generate the corresponding mononuclear Cu^I sites. T4 and T10 sites were not included because they are located in the distorted 6-membered rings inside the wall of the sinusoidal channel.[22,42,43] However, these two T sites were included in the models for the local environment of the Cu^I binding sites. For geometry optimization and transition state searches, 18 Si atoms were constrained at their crystallographically defined coordinates.[23,43] The relative energies of the different binuclear $Cu^{I/II}$ sites and the mononuclear Cu^I sites (20 total) that make up the 10 binuclear Cu^I sites have been corrected for differences in the strain energies of their respective lattice environments. The strain energies are evaluated by calculating the energies of the models without Cu ions and subtracting these energies from the total energies of the $[Cu_2O]^{2+}$, mononuclear, and binuclear Cu^I models. Spin-unrestricted DFT calculations were performed on these models with Gaussian 09[44] and the B3LYP functional.[45−47] For all calculations, a 6-311G* basis set was used on the Cu−O−Cu core atoms, the Cu-coordinating lattice oxygen atoms, and N_2O. A 6-31G* basis set was used for all other atoms. We previously employed an identical theoretical approach in computational modeling of the spectroscopic features of the bent mono-μ-oxo core in Cu−ZSM-5.[13] This approach was found to well reproduce the spectroscopic and thermodynamic properties of the reactive intermediate. Broken symmetry calculations were performed for all singlet spin states. Mulliken population analyses[48] and Mayer bond order (MBO) analyses[49] were performed with QMForge,[50] and vibrations and molecular orbitals were visualized in Avogadro.[51]

3. RESULTS AND ANALYSIS

3.1. Nature of Binuclear Cu^I Active Sites. As the $[Cu_2O]^{2+}$ site in Cu−ZSM-5 has been spectroscopically characterized, its spectral features (i.e., the symmetric and antisymmetric Cu−O−Cu vibrational frequencies and the energy of the oxo → Cu^{II} charge transfer (CT) transition) allow for experimental calibration of DFT structural models for investigating the nature of the corresponding binuclear Cu^I site capable of forming the $[Cu_2O]^{2+}$ species.[13] As only one set of RR vibrations is present, only one $[Cu_2O]^{2+}$ species is found in the N_2O and O_2 reactions. There are 10 possible pairs of binuclear Cu sites separated by two Si T units within the 10-membered rings of ZSM-5. From these possible pairs, 10 $[Cu_2O]^{2+}$ sites were constructed and geometry optimized. Their calculated geometric and spectral features are listed and compared to experiment in Table 1 and Figure S1B, Supporting Information. The corresponding binuclear Cu^I sites were obtained by removing the bridging oxo and subsequent

Table 1. Comparison between the Experimental and the Calculated oxo → Cu^{II} Charge Transfer Transition, Symmetric/Antisymmetric Cu−O−Cu Vibrational Modes, and Cu−O−Cu Angle of the $[Cu_2O]^{2+}$ Core[a]

	oxidized form ($[Cu_2O]^{2+}$)			reduced form ($Cu^I\cdots Cu^I$)	
	∠Cu−O−Cu (deg)	$\nu_{sym}/\nu_{antisym}$ (cm^{-1})	$CT_{oxo\ to\ Cu}$ (cm^{-1})	binding types	$d_{Cu\cdots Cu}$ (Å)
exp.	**139**	**456/870**	**22 700**	**2 or 3 CN**	**4.43**
site 1	134	445/855	23 159	II,III	4.56
site 2	143	426/857	23 502	II,III	5.03
site 3	146	407/784	21 693	I,I	4.14
site 4	144	417/850	22 280	II,III	5.02
site 5	133	447/859	22 617	I,I	2.48
site 6	**135**	**451/842**	**22 926**	III,III	4.17
site 7	145	415/856	21 300	II,III	5.85
site 8	147	391/860	22 841	I,III	3.54
site 9	145	419/843	21 077	I,III	3.57
site 10	145	408/815	22 897	I,III	4.76

[a]Also included are the structures of their corresponding binuclear Cu^I sites.

dx.doi.org/10.1021/ja4113808 | J. Am. Chem. Soc. 2014, 136, 3522−3529

geometry optimization as described in the Materials and Methods. The calculated structures of the $2Cu^{I}$ sites are also included in Table 1 and shown in Figure S2, Supporting Information. The relative energies of the different binuclear $Cu^{I/II}$ sites have been corrected for differences in the strain energies of their respective lattice environments (see Materials and Methods).

All Cu^{II} centers in the 10 $[Cu_2O]^{2+}$ sites are bound by two lattice oxygens of Al T sites with $\angle O_{lat}-Cu-O_{lat}$ bite angles of ~80° (Figure S1, Supporting Information). The range in relative energies of these triplet $[Cu_2O]^{2+}$ sites is ~15 kcal/mol (Figure 1A, left). Note that both the broken symmetry singlet and triplet states of the 10 $[Cu_2O]^{2+}$ sites were evaluated and have nearly identical geometries and energies (within 1 kcal/mol). In contrast to the very similar binding modes for the $[Cu_2O]^{2+}$ sites, which result in their relatively tight energy range, the binding modes of the Cu^{I} centers to lattice oxygens are variable. This variability in copper binding results in a large energy range for their corresponding binuclear Cu^{I} sites (~40 kcal/mol) (Figure 1A, right). To further explore the origin of the large energy span of the binuclear Cu^{I} sites, the energies of the mononuclear Cu^{I} sites (20 total; 10 are redundant) that make up the 10 binuclear Cu^{I} sites were also evaluated. On the basis of the structures and energies of these mononuclear Cu^{I} sites, three general binding modes of the Cu^{I} centers to lattice oxygen are elucidated, with each type of binding mode having a limited energy range (Figure 1B). Binding mode I consists of two-coordinate, mononuclear Cu^{I} sites with small bite angles (~80°); both ligands are Al T-site lattice oxygens. Binding mode II consists of three-coordinate Cu^{I} sites. Two ligands are Al T-site lattice oxygens, while a third is a Si T-site lattice oxygen. Cu^{I} sites with binding mode III are two coordinate with more linear bite angles (~149°). One lattice oxygen ligand is from an Al T site, and the other is from a Si T site. Binding modes I and II have similar energies and are at least 3 kcal/mol higher in energy than those of binding mode III. Binding modes I and III have differences in both the chemical nature of their lattice oxygen atoms and their bite angle. In order to decouple these two contributions to their relative energies, an additional model was constructed (hypothetical binding mode IV, Figure 1B). In this model, the adjacent positions of Si and Al in binding mode III were rearranged to construct a model with two O_{Al} donor ligands to one Cu^{I} center. While the bite angles of binding modes III ($1O_{Al}$ + $1O_{Si}$) and IV ($2O_{Al}$) are the same, the latter is 11 kcal/mol lower in energy due to the polarization of the coordinated lattice oxide of the Al T sites. Binding modes I (∠O−Cu−O ~80°) and IV (∠O−Cu−O ~149°) both have the same chemical nature of the lattice oxygen ligation ($2O_{Al}$). The more linear bite angle of binding mode IV significantly stabilizes Cu^{I} binding relative to the bent bite angle of binding mode I by 24 kcal/mol (Figure 1B). The linear Cu^{I} geometry provided by the ZSM-5 lattice is thus responsible for the significant relative stability of binding mode III sites. Note that the two strongest Cu−O bonds in binding mode II have relatively bent bite angles (∠O−Cu−O 82−142°) as compared to binding mode III, which results in their having higher energies.

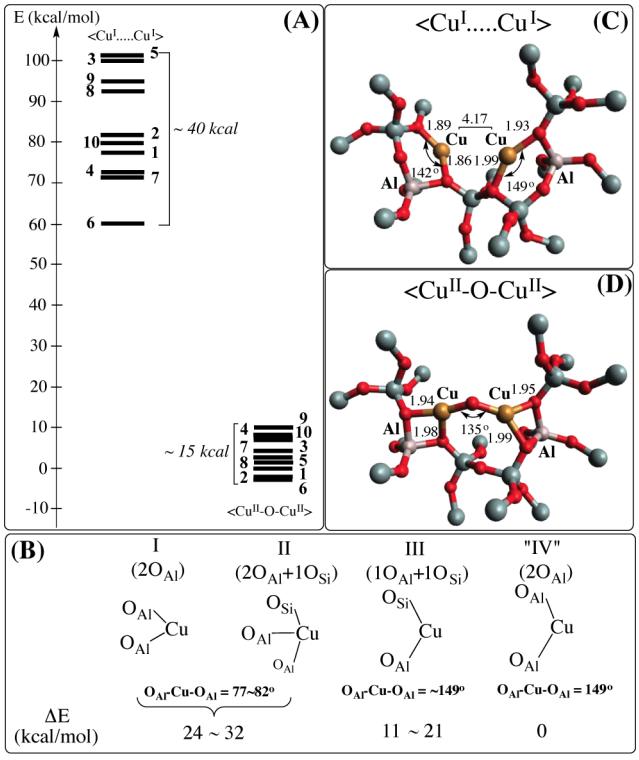

Figure 1. (A) Relative energies of the 10 $[Cu_2O]^{2+}$ (right) and binuclear Cu^{I} sites (left) separated by 2 Si T sites. (B) Structures and relative energies of three representative Cu^{I} binding modes and the hypothetical mode (IV) in the Cu−ZSM-5 lattice. (C) DFT model for the binuclear Cu^{I} site 6. (D) Spectroscopically calibrated DFT model for the $[Cu_2O]^{2+}$ site. Note that the Si atoms are given in gray, and hydrogen atoms are omitted in C and D for clarity.

From Table 1, we assign the $[Cu_2O]^{2+}$ site observed experimentally to site 6 based on comparison of the calculated spectral features of the 10 different geometry optimized pairs of $[Cu_2O]^{2+}$ sites and the energies of their corresponding $2Cu^{I}$ reduced sites. The oxidized and reduced structures are given in Figure 1C and 1D, respectively. Specifically, for the $[Cu_2O]^{2+}$ core structures, sites 1, 5, and 6 have similar calculated spectral features that are in agreement with experiment; however, the reduced site 6 is at least 12 kcal/mol lower in energy than all other binuclear Cu^{I} sites. This large energy range of binuclear Cu^{I} sites and the significant energetic stabilization of one reduced structure over all others would be consistent with preferential population under autoreducing conditions at elevated temperature (~450 °C).[25] As shown in Figure 1D, the Cu^{I} centers of site 6 are stabilized by two type III binding modes with a 4.17 Å $Cu^{I}-Cu^{I}$ distance, minimizing the electrostatic repulsion between the two Cu^{I} ions. The Cu−O−Cu angle of the $[Cu_2O]^{2+}$ core in this site is calculated to be 135°, similar to the 139° angle obtained from a normal coordinate analysis (NCA) of the symmetric/antisymmetric Cu−O−Cu stretching frequencies and their isotope perturbations. Note that the 2 Al T units of site 6 are located at the intersection of straight and sinusoidal 10-membered rings channels. This site has previously been associated with a 540 nm luminescence band and also correlates with the catalytic activity in NO decomposition.[19,20,22,24]

3.2. Mechanism of $[Cu_2O]^{2+}$ Core Formation from N_2O.

The experimental rate of formation of the $[Cu_2O]^{2+}$ core in the ZSM-5 lattice from reaction of $N_2O_{(g)}$ with autoreduced Cu−ZSM-5 can be monitored by the growth of its characteristic 22 700 cm^{-1} absorption band. In order to determine the E_a for this reaction the rate of $[Cu_2O]^{2+}$ formation was measured at six different temperatures from 25 to 100 °C. Data were fit to the Arrhenius equation, where the plot of $\ln(k)$ against $1/T$ has a

dx.doi.org/10.1021/ja4113808 | J. Am. Chem. Soc. 2014, 136, 3522−3529

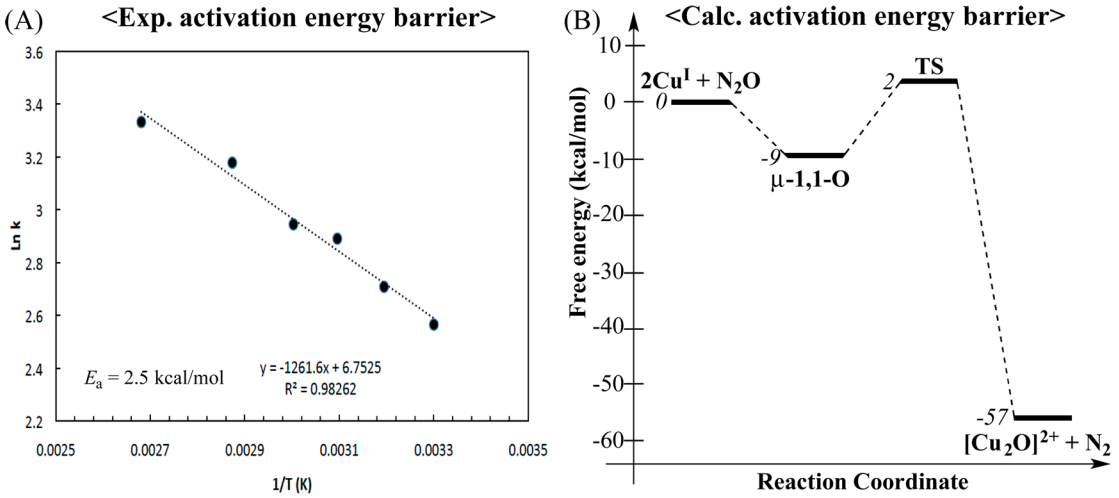

Figure 2. (A) Apparent (i.e., observed) E_a measured from the temperature dependence of the formation of the 22 700 cm^{-1} absorption band upon reaction of autoreduced Cu−ZSM-5 with $N_2O_{(g)}$. (B) Calculated reaction coordinate for N_2O activation by the binuclear Cu^I site 6 via the μ-1,1-O reactant complex.

slope of $-E_a/RT$. The experimentally derived E_a for $[Cu_2O]^{2+}$ formation from $N_2O_{(g)}$ is thus determined to be 2.5 ± 0.5 kcal/mol (Figure 2A; see Figure S4, Supporting Information, for the $\ln(Abs_0 - Abs_f)/Abs_t - Abs_f)$ vs time plots and fits). Note that the experimental activation energy includes the heat of adsorption of N_2O and is thus an apparent value that is decreased from the value for N−O cleavage.

As indicated in section 3.1, site 6 corresponds to both the $[Cu_2O]^{2+}$ core associated with the experimental data on the intermediate and the lowest energy binuclear Cu^I site. We therefore used site 6 to study the reaction of N_2O with the binuclear Cu^I site to form the $[Cu_2O]^{2+}$ core and to correlate to the experimental E_a. Three possible N_2O binding modes (i.e., η^1-N, μ-1,1-O, μ-1,3-O,N, Scheme 1) to the binuclear Cu^I site 6

Scheme 1. Three N_2O Binding Modes on the Binuclear Cu^I Center of Site 6

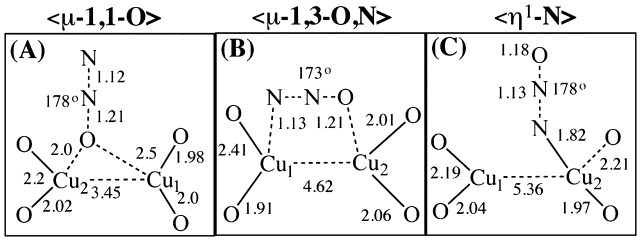

were evaluated. N_2O binding is found to be exothermic in all cases (Table 2), with a stabilization energy of ∼11 ± 2 kcal/mol (9 kcal/mol for the μ-1,1-O structure in Figure 2B). The σ-donor and π back-bonding interactions between N_2O and the Cu^I center(s) can be quantified by (1) the total amount of N_2O occupied molecular orbitals mixed into the unoccupied Cu 4s and 4p orbitals and (2) the amount of occupied Cu 3d character in the unoccupied N_2O π^* orbitals, respectively. The σ-donor and π back-bonding interactions are given in Table 2. The total σ/π contributions are found to be quite similar, consistent with their similar binding energies.

The PES for elongation of the N−O bond was first calculated to estimate the activation energy barrier for formation of the $[Cu_2O]^{2+}$ intermediate from each of these N_2O binding modes. Formation of a $[Cu_2O]^{2+}$ site via the most stable η^1-N binding

Table 2. Relative Binding Energies and Their σ-Donor/π Back-Bonding Interactions of the Three N_2O Binding Modes for the Binuclear Cu^I Site 6 in Cu−ZSM-5

	site 6		
binding modes	μ-1,1-O	η^1-N	μ-1,3-O,N
binding energy[a]	−9	−13	−11
E_a[a]	2	>60	5
N−N−O angle	178	178	173
σ-donor[b]	7	5	5
π back-bonding[c]	3	6	9

[a]kcal/mol. [b]The percent contribution of computed N_2O bonding contribution mixed into the unoccupied Cu 4s and 4p orbitals [c]The percent contribution of computed Cu 3d orbitals contribution mixed into the unoccupied N_2O π^* orbitals

mode is computationally excluded due the lack of a proper reaction coordinate to form an oxo bridge to two Cu centers and the fact that N−O bond cleavage in this model leads to a high-energy, noncoordinated O^{2-} species (>60 kcal/mol). Although similar to the μ-1,3-O,N binding mode, the calculated activation energy via a μ-1,1-O reactant complex is the lowest among the three possible binding modes (11 kcal/mol, Table 2 and Figure S5, Supporting Information). This gives an apparent activation energy of 2 kcal/mol (Figure 2B), which is consistent with the experimental activation energy (Figure 2A). Thus, the mechanism of the formation of the $[Cu_2O]^{2+}$ site from μ-1,1-O-bound N_2O will be considered below. The calculated activation mechanism of the μ-1,3-O,N binding mode is similar to μ-1,1-O and given in Figure S4, Supporting Information.

Both singlet and triplet PESs for cleavage of the N−O bond from the μ-1,1-O binding mode were evaluated to determine the contributions of the different spin states to N_2O activation. At a fixed N−O bond distance of the singlet reactant complex (d_{N-O} 1.21 Å), the triplet state is 22 kcal/mol higher in energy and the ∠N−N−O is significantly bent (∼121° compared to ∼178° for the singlet) (Figure 3A). The triplet surface is dissociative for N−O bond cleavage, and the first crossing point between the singlet and triplet PESs in Figure 3A is at an N−O distance of ∼1.35 Å. However, at this point, ∠N−N−O of singlet and triplet geometries are different (singlet 169°; triplet 125°). Alternatively, there is another crossing point at an N−O

dx.doi.org/10.1021/ja4113808 | J. Am. Chem. Soc. 2014, 136, 3522−3529

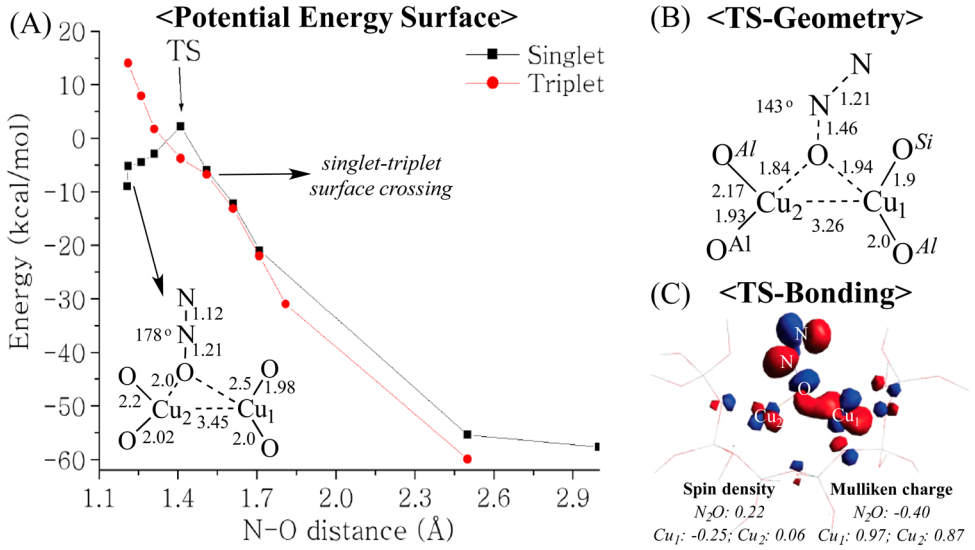

Figure 3. (A) Singlet and triplet N−O cleavage potential energy surfaces for site 6. (B) Transition state geometry on the singlet potential energy surface. (C) Transition state spin density and Mulliken charge analyses, and representative molecular orbital contour associated with the bonding between the two Cu centers and of the N_2O π^* orbital (HOMO-1 of α-spin levels).

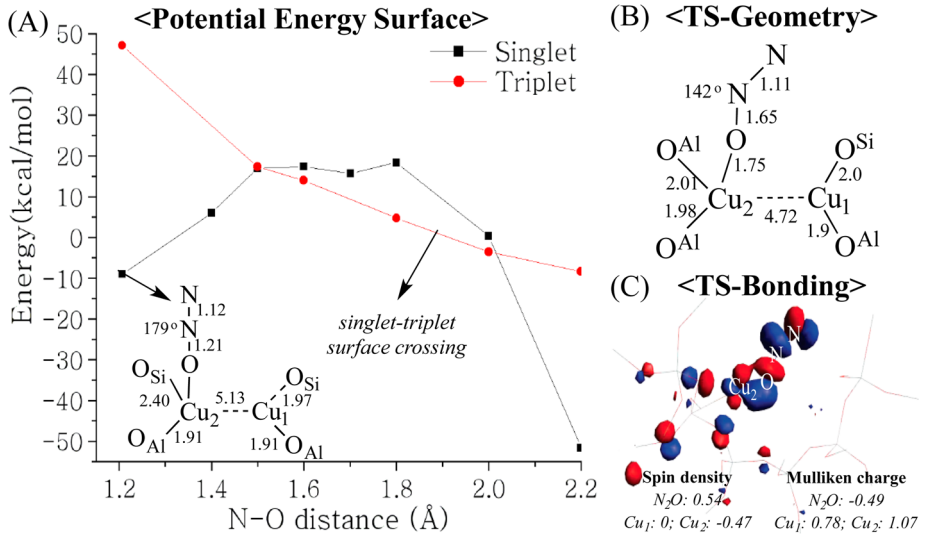

Figure 4. (A) Singlet and triplet N−O potential energy surfaces for site 7. (B) Transition state geometry on the singlet potential energy surface. (C) Transition state spin density, Mulliken charges, and molecular orbital contour associated with the bonding interaction between the two Cu centers and N_2O π^* orbital (HOMO-9 of α-spin levels).

distance of ∼1.55 Å. Here, the geometric and electronic structures of the singlet and triplet models are very similar (∠N−N−O ≈ 122°), and therefore, this corresponds to the minimum energy crossing point (MEXP). Importantly, the MEXP takes place after the activation energy barrier on the singlet surface (Figure 3A, N−O distance ≈ 1.55 Å, ∠N−N−O ≈ 124°), and thus, N_2O activation proceeds on this surface. A transition state structure on the singlet surface was obtained and confirmed to have one imaginary frequency. This transition state is on the intrinsic reaction coordinate (IRC) to both the μ-1,1-O reactant and the $[Cu_2O]^{2+}$ product. In going from the reactant complex to the transition state, the Cu−O_{N2O} bonds become stronger and more symmetric to the two Cu centers (reactant complex Cu_1−O_{N2O} 2.5 Å, Cu_2−O_{N2O} 2.0 Å; transition state Cu_1−O_{N2O} 1.94 Å, Cu_2−O_{N2O} 1.84 Å) (Figure 3B).

The change in Mulliken charges on the N_2O fragment (reactant 0.04; TS −0.40; $[Cu_2O]^{2+}$ product −0.93) and the N−O Mayer bond orders (reactant 1.25; TS 0.71; product 0) demonstrate that the transition state is best described as involving a one-electron transfer from Cu_1 to a low-lying π^* orbital of N_2O. The reaction is completed by the second electron transfer from Cu_2 and cleavage of the N−O bond to form the $[Cu_2O]^{2+}$ site and N_2 (Figure S5, Supporting Information). Although the bond distances of O_{N2O} between two Cu centers are not significantly different at the transition state, the spin density distribution (Cu_1 −0.25; Cu_2 0.06; N_2O 0.22) indicates that the electron is predominately transferred from Cu_1 to N_2O rather than evenly transferred from the two Cu centers. This reflects the well-orientated overlap between the Cu_1-occupied 3d orbital and the low-lying π^* orbital of the bent N_2O (∠N−N−O ≈ 143°), which can be observed in the molecular orbital contour (α-orbital HOMO-1) (Figure 3C).

dx.doi.org/10.1021/ja4113808 | J. Am. Chem. Soc. 2014, 136, 3522−3529

The bent N−N−O angle preferentially stabilizes one of the unoccupied N_2O π^* orbitals and facilitates the back-bonding interaction between Cu_1 and N_2O at the transition state.

3.3. Geometric Requirements for $[Cu_2O]^{2+}$ Active Site Formation. Our previous RR study showed that only one $[Cu_2O]^{2+}$ site is formed via N_2O and O_2 activation.[13] As the binuclear Cu^I sites 7 and 4 are only ∼12 kcal/mol higher in energy than site 6, $[Cu_2O]^{2+}$ core formation at these sites was also evaluated. These sites both have one type II and one type III Cu^I center (Figure 1B and Figure S2, Supporting Information), and N_2O preferentially coordinates to the type II Cu^I site in an η^1-O or η^1-N fashion (i.e., nonbridging) (Figures S6 and S7, Supporting Information). Binding via η^1 coordination rather than bridging in these binuclear sites is attributed to their longer Cu^I−Cu^I distances (site 7 5.85 Å; site 4 5.02 Å). As both sites 7 and 4 have similar energies and a similar N_2O binding mode, site 7 was used to evaluate the activation energy for N_2O formation of the $[Cu_2O]^{2+}$ core.

Reaction of site 7 with N_2O also proceeds along the singlet surface (Figure 4). On the basis of the Mulliken charge on the N_2O fragment (reactant 0.05; TS −0.49; product −0.88) and N−O Mayer bond order (reactant 1.27; TS 0.49; product 0), the transition state again involves one-electron transfer from Cu to the N_2O π^* molecular orbital (Figure 4C and Figure S8, Supporting Information). However, the calculated E_a of site 7 (Figure 4A) is significantly higher than that of site 6 (site 6, 2 kcal/mol; site 7, 16 kcal/mol) and has a later transition state in terms of N−O bond distance (site 6, 1.46 Å; site 7, 1.65 Å). The significantly lower E_a for site 6 relative to site 7 is due to the additional stabilization of the transition state through the bridged bonding to the second Cu (Figure 3B). However, in site 7, N_2O remains essentially η^1-O bound to one Cu at the transition state (Figure 4B). Note that for site 7 as the N−O bond distance elongates past the transition state (∼2.2 Å), the η^1-O oxo atom eventually forms a bridge to the other Cu ion (μ-1,1-O), which results in transfer of the second electron to form the $[Cu_2O]^{2+}$ product (Figure 4A right). The large E_a for site 7 and thus its inability to activate N_2O is consistent with experiment in that N_2O reacts selectively with a specific pair of Cu^I ions. Therefore, the lack of additional $[Cu_2O]^{2+}$ species in the 10-membered rings of ZSM-5 mainly results from this kinetic barrier. The large E_a prohibits N_2O activation via an η^1-O nonbridged binding mode, which would also be the situation for any potentially present mononuclear Cu^I site or binuclear Cu^I sites with relatively long Cu^I−Cu^I distances. The significantly higher activation energy for formation $[Cu_2O]^{2+}$ species from a terminal N_2O-bound Cu^I center rationalizes the experimental observations that Cu−zeolites with low Cu/Al ratios (i.e., fewer Cu−Cu pairs) generate fewer $[Cu_2O]^{2+}$ active cores and have much lower N_2O decomposition activity, irrespective of structural type. In fact, with low Cu/Al ratios that do not form any $[Cu_2O]^{2+}$ active core, the activity for N_2O decomposition is indeed zero.[10,52] Thus, in Cu−ZSM-5, the low E_a for N_2O activation is facilitated by the ability to bridge the N_2O to two Cu^I centers. This bridged binding stabilizes the Cu^{II}−N_2O^{1-}−Cu^I species in the transition state while facilitating the second electron transfer required for N−O bond cleavage.

4. DISCUSSION

Guided by spectroscopically validated DFT calculations, the geometric and electronic structural criteria for binuclear Cu^I sites in Cu−ZSM-5 to activate N_2O have been elucidated. The mechanism of N_2O activation and subsequent formation of the $[Cu_2O]^{2+}$ active core have also been evaluated. While three Cu^I/lattice-oxygen binding modes have been identified, site 6, with two type III Cu^I centers (Figure 1B), is the most stable structure (by >12 kcal/mol relative to other $2Cu^I$ sites) and should have a significant population among the possible pairs of Cu^I sites within the 10-membered rings of ZSM-5. Site 6 also has the lowest calculated E_a (also in agreement with experiment) for formation of the $[Cu_2O]^{2+}$ core from N_2O. Generation of other $[Cu_2O]^{2+}$ sites from higher energy binuclear Cu^I sites was found to be kinetically unfavorable due to their significantly larger E_as (16 vs 2 kcal/mol). This is due to the longer $Cu^I\cdots Cu^I$ distances in these nonreactive sites, which preclude N_2O bridging to both Cu's in a μ-1,1-O fashion. These results provide both thermodynamic and kinetic rational for the presence of only one $[Cu_2O]^{2+}$ site in N_2O-activated Cu−ZSM-5.

The formation mechanism of the $[Cu_2O]^{2+}$ site via N_2O activation from the binuclear Cu^I site 6 indicates that N_2O is activated along the singlet potential energy surface. The transition state is described as a one-electron transfer from one Cu^I center into the N_2O π^* orbital, which is stabilized in energy due to its bent N−N−O structure.[31] E_a for N_2O activation on a single Cu^I center with a terminal η^1-O binding mode is significantly higher, indicating that N_2O bridging two Cu centers is essential for a low E_a. Bridging two Cu's also facilitates the second electron transfer required for N−O bond cleavage to form the $[Cu_2O]^{2+}$ core.

As mentioned in the Introduction, Cu−ZSM-5 is not the only system that activates N_2O at a multi-Cu center. In biology, the N_2O to N_2 conversion is a key step in bacterial denitrification and catalyzed by a tetranuclear Cu cluster in the enzyme N_2OR. Recent research has identified two forms of the tetranuclear Cu_Z site: a [4Cu:S] cluster (Cu_Z*) and a [4Cu:2S] cluster (Cu_Z).[27,29] A recent study has determined that Cu_Z* is the catalytically relevant form.[53] Two factors give rise to the high reactivity of the Cu_Z* cluster in N_2OR: (1) formation of a fully reduced ($4Cu^I$) cluster and (2) an open coordination position on a Cu^I,Cu^{IV} edge for reaction with N_2O to form an oxo-bridged product. This important finding, in combination with the results presented here on Cu−ZSM-5, allows us to directly compare similarities and differences in the mechanism of N_2O activation as carried out by binuclear Cu^I sites in biological and heterogeneous systems. While both have $2Cu^I$ reactive centers, the donor ligand set in Cu_Z* involves protein-derived His residues and an inorganic μ_4-sulfide, while in Cu−ZSM-5 the Cu's are bound to either Si−O or Al−O bonds provided by the zeolite lattice T sites (Scheme 2). As discussed below, these structural differences result in differences in the thermodynamic and kinetic aspects of their reaction mechanisms.

Scheme 2. Product of N_2O Reduction by (A) N_2OR and (B) Cu−ZSM-5

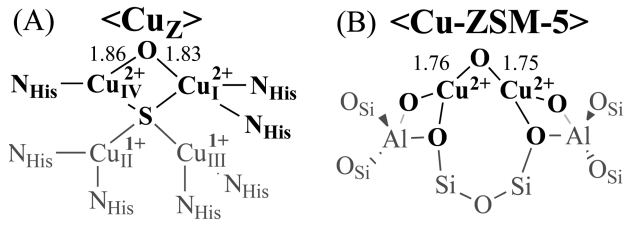

dx.doi.org/10.1021/ja4113808 | J. Am. Chem. Soc. 2014, 136, 3522−3529

Similar to previous studies related to N_2OR, the μ-1,1-O and μ-1,3-O,N binding modes of the $2Cu^I$ site 6 in Cu−ZSM-5 have similar E_as.[30,31,54] However, the calculated activation energy barrier for N_2O cleavage in N_2OR is significantly higher than that for Cu−ZSM-5 (Cu−ZSM-5 5 kcal/mol, N_2OR 14 kcal/mol) (Figure S4, Supporting Information). The higher E_a for the Cu_Z site in N_2OR is reflected in the later transition state in terms of N−O distance and ∠N−N−O angle (N_2OR d_{N-O} = 1.9 Å;, ∠N−N−O = 110°; Cu−ZSM-5 d_{N-O} = 1.64 Å, ∠N−N−O = 120°) (Table 3). The earlier transition state in Cu−ZSM-5 results from the larger thermodynamic driving force (N_2OR −33 kcal/mol; Cu−ZSM-5 −57 kcal/mol) for oxo transfer. The increased driving force in Cu−ZSM-5 is derived from the stronger $Cu-O_{oxo}$ bonds in the $[Cu_2O]^{2+}$ product relative to those in oxo-bridged N_2OR ($d(Cu-O_{oxo})$ 1.75 Å in Cu−ZSM-5; $d(Cu-O_{oxo})$ 1.85 Å in N_2OR). This is further supported by their similar intrinsic activation energies (i.e., corrected for free energy differences between the reactants and products) (N_2OR 28 kcal/mol; Cu−ZSM-5 25 kcal/mol) obtained from the Marcus relationship.[55] The stronger $Cu-O_{oxo}$ bonds in Cu−ZSM-5 relative to N_2OR are due the differences in the donor ligand sets mentioned above, that is, the two lattice oxide ligands in Cu−ZSM-5 have a reduced donor interaction with Cu relative to the μ_4-sulfide and histidine ligands in N_2OR (Scheme 2).

Table 3. Calculated Activation Barrier (E_a), Intrinsic Barrier ($\Delta G_0^{\ddagger}$), Thermodynamic Driving Force (ΔG_{rxn}) (kcal/mol), and Metrical Parameters for the Transition State Geometries in Cu−ZSM-5 and N_2OR (μ-1,3-O,N binding mode)[31]

μ-1,3-O,N	E_a	$\Delta G_0^{\ddagger}$	ΔG_{rxn}	$d_{N-O\ (N2O)}$	∠N−N−O
Cu−ZSM-5	5	25	−57	1.64	120°
N_2OR	14	28	−33	1.90	110°

In summary, this study demonstrates that Cu^I centers in the ZSM-5 framework prefer two-coordinate binding to Al T-site lattice O's with a close to linear bite angle. The two Cu^I centers must be close enough to allow N_2O to bridge in either a μ-1,1-O or a μ-1,3-N_2O structure. These binding modes result in a low activation energy barrier for oxo transfer and formation of the $[Cu_2O]^{2+}$ site. The geometric and electronic structure requirements of the binuclear Cu^I sites and the formation mechanism of the $[Cu_2O]^{2+}$ core in Cu−ZSM-5 provide new insights into Cu−zeolite sites capable of N_2O (and O_2) activation. These insights assist in the development of general strategies to activate the thermodynamically stable and chemically inert N_2O molecule to reduce its greenhouse contribution and enable its utilization as a precursor to valuable chemical feedstocks.

■ ASSOCIATED CONTENT

Supporting Information

Full listing of authors for ref 44; calculated $[Cu_2O]^{2+}$ and binuclear Cu^I DFT models for the other 9 possible pairs; schematic representations of η^1-N_2O binding modes for sites 7 and site4; spin densities, Mulliken charges, and Mayer bond order analyses for site 6 with μ-1,1-O/μ-1,3-O,N N_2O binding modes and for site 7 with a η^1-O binding mode along the N−O singlet potential energy surface. This material is available free of charge via the Internet at http://pubs.acs.org.

■ AUTHOR INFORMATION

Corresponding Authors

bert.sels@biw.kuleuven.be
robert.schoonheydt@biw.kuleuven.be
edward.solomon@stanford.edu

Notes

The authors declare no competing financial interest.

■ ACKNOWLEDGMENTS

This work was supported by National Science Foundation Grant CHE-0948211 (to E.I.S.) and funded within the framework of FWO (G.0596.11), IAP (Belspo), ERIC, Methusalem (long-term structural funding by the Flemish Government) projects. We acknowledge Mrs. Esther Johnston for carefully reading the manuscript. M.-L.T. received support from the Postdoctoral Research Abroad Program sponsored by the National Science Council, Taiwan (R.O.C.), and R.G.H. acknowledges a Gerhard Casper Stanford Graduate Fellowship and Achievement Rewards for College Scientists (ARCS) Foundation

■ REFERENCES

(1) Arakawa, H.; Aresta, M.; Armor, J. N.; Barteau, M. A.; Beckman, E. J.; Bell, A. T.; Bercaw, J. E.; Creutz, C.; Dinjus, E.; Dixon, D. A.; Domen, K.; DuBois, D. L.; Eckert, J.; Fujita, E.; Gibson, D. H.; Goddard, W. A.; Goodman, D. W.; Keller, J.; Kubas, G. J.; Kung, H. H.; Lyons, J. E.; Manzer, L. E.; Marks, T. J.; Morokuma, K.; Nicholas, K. M.; Periana, R.; Que, L.; Rostrup-Nielson, J.; Sachtler, W. M.; Schmidt, L. D.; Sen, A.; Somorjai, G. A.; Stair, P. C.; Stults, B. R.; Tumas, W. *Chem. Rev.* **2001**, *101*, 953.

(2) Conley, B. L.; Tenn, W. J.; Young, K. J. H.; Ganesh, S.; Meier, S.; Ziatdinov, V.; Mironov, O.; Oxgaard, J.; Gonzales, J.; Goddard, W. A.; Periana, R. A. *Activation of Small Molecules*; Weinheim: Germany, 2006, p 235.

(3) Hansen, J. B.; Højlund Nielsen, P. E. *Handbook of Heterogeneous Catalysis*; Weinheim: Germany, 2008.

(4) Himes, R. A.; Karlin, K. D. *Proc. Natl. Acad. Sci.* **2009**, *106*, 18877.

(5) Himes, R. A.; Barnese, K.; Karlin, K. D. *Angew. Chem., Int. Ed.* **2010**, *49*, 6714.

(6) Groothaert, M. H.; Smeets, P. J.; Sels, B. F.; Jacobs, P. A.; Schoonheydt, R. A. *J. Am. Chem. Soc.* **2005**, *127*, 1394.

(7) Smeets, P. J.; Groothaert, M. H.; Schoonheydt, R. A. *Catal. Today* **2005**, *110*, 303.

(8) Groothaert, M. H.; Lievens, K.; Leeman, H.; Weckhuysen, B. M.; Schoonheydt, R. A. *J. Catal.* **2003**, *220*, 500.

(9) Groothaert, M. H.; Van, B. J. A.; Battiston, A. A.; Weckhuysen, B. M.; Schoonheydt, R. A. *J. Am. Chem. Soc.* **2003**, *125*, 7629.

(10) Smeets, P. J.; Groothaert, M. H.; van, T. R. M.; Leeman, H.; Hensen, E. J. M.; Schoonheydt, R. A. *J. Catal.* **2007**, *245*, 358.

(11) Groothaert, M. H.; Lievens, K.; Leeman, H.; Weckhuysen, B. M.; Schoonheydt, R. A. *J. Catal.* **2003**, *220*, 500.

(12) Smeets, P. J.; Groothaert, M. H.; van Teeffelen, R. M.; Leeman, H.; Hensen, E. J. M.; Schoonheydt, R. A. In *Studies in Surface Science and Catalysis*; Ruren Xu, Z. G. J. C., Wenfu, Y., Eds.; Amsterdam: The Netherlands, 2007; Vol. *170*, p 1080.

(13) Woertink, J. S.; Smeets, P. J.; Groothaert, M. H.; Vance, M. A.; Sels, B. F.; Schoonheydt, R. A.; Solomon, E. I. *Proc. Natl. Acad. Sci. U.S.A.* **2009**, *106*, 18908.

(14) Karlin, K. D.; Gultneh, Y.; Hayes, J. C.; Zubieta, J. *Inorg. Chem.* **1984**, *23*, 519.

(15) Smeets, P. J.; Woertink, J. S.; Sels, B. F.; Solomon, E. I.; Schoonheydt, R. A. *Inorg. Chem.* **2010**, *49*, 3573.

(16) Bordiga, S.; Groppo, E.; Agostini, G.; van Bokhoven, J. A.; Lamberti, C. *Chem. Rev.* **2013**, *113*, 1736.

(17) Vanelderen, P.; Vancauwenbergh, J.; Sels, B. F.; Schoonheydt, R. A. *Coord. Chem. Rev.* **2013**, *257*, 483.

(18) Dedecek, J.; Wichterlova, B. *J. Phys. Chem.* **1994**, *98*, 5721.
(19) Nachtigallova, D.; Nachtigall, P.; Sauer, J. *Phys. Chem. Chem. Phys.* **2001**, *3*, 1552.
(20) Lamberti, C.; Bordiga, S.; Salvalaggio, M.; Spoto, G.; Zecchina, A.; Geobaldo, F.; Vlaic, G.; Bellatreccia, M. *J. Phys. Chem. B* **1997**, *101*, 344.
(21) Nachtigall, P.; Nachtigallová, D.; Sauer, J. *J. Phys. Chem. B* **2000**, *104*, 1738.
(22) Nachtigallova, D.; Nachtigall, P.; Sierka, M.; Sauer, J. *Phys. Chem. Chem. Phys.* **1999**, *1*, 2019.
(23) Mentzen, B. F.; Bergeret, G. *J. Phys. Chem. C* **2007**, *111*, 12512.
(24) Dedecek, J.; Wichterlova, B. *Phys. Chem. Chem. Phys.* **1999**, *1*, 629.
(25) Smeets, P. J.; Hadt, R. G.; Woertink, J. S.; Vanelderen, P.; Schoonheydt, R. A.; Sels, B. F.; Solomon, E. I. *J. Am. Chem. Soc.* **2010**, *132*, 14736.
(26) Zumft, W. G. *Microbiol. Mol. Biol. Rev.* **1997**, *61*, 533.
(27) Wust, A.; Schneider, L.; Pomowski, A.; Zumft, W. G.; Kroneck, P. M.; Einsle, O. *Biol. Chem.* **2012**, *393*, 1067.
(28) Brown, K.; Tegoni, M.; Prudencio, M.; Pereira, A. S.; Besson, S.; Moura, J. J.; Moura, I.; Cambillau, C. *Nat. Struct. Biol.* **2000**, *7*, 191.
(29) Pomowski, A.; Zumft, W. G.; Kroneck, P. M. H.; Einsle, O. *Nature* **2011**, *477*, 234.
(30) Chen, P.; DeBeer George, S.; Cabrito, I.; Antholine, W. E.; Moura, J. J.; Moura, I.; Hedman, B.; Hodgson, K. O.; Solomon, E. I. *J. Am. Chem. Soc.* **2002**, *124*, 744.
(31) Gorelsky, S. I.; Ghosh, S.; Solomon, E. I. *J. Am. Chem. Soc.* **2006**, *128*, 278.
(32) Tolman, W. B. *Angew. Chem., Int. Ed.* **2010**, *49*, 1018.
(33) Haack, P.; Kärgel, A.; Greco, C.; Dokic, J.; Braun, B.; Pfaff, F. F.; Mebs, S.; Ray, K.; Limberg, C. *J. Am. Chem. Soc.* **2013**, *135*, 16148.
(34) Coperet, C. *Chem. Rev.* **2009**, *110*, 656.
(35) Haack, P.; Limberg, C.; Ray, K.; Braun, B.; Kuhlmann, U.; Hildebrandt, P.; Herwig, C. *Inorg. Chem.* **2011**, *50*, 2133.
(36) Ertem, M.; Cramer, C.; Himo, F.; Siegbahn, P. M. *J. Biol. Inorg. Chem.* **2012**, *17*, 687.
(37) Bar-Nahum, I.; Gupta, A. K.; Huber, S. M.; Ertem, M. Z.; Cramer, C. J.; Tolman, W. B. *J. Am. Chem. Soc.* **2009**, *131*, 2812.
(38) Wischert, R.; Laurent, P.; Copéret, C.; Delbecq, F.; Sautet, P. *J. Am. Chem. Soc.* **2012**, *134*, 14430.
(39) Iwamoto, M.; Furukawa, H.; Mine, Y.; Uemura, F.; Mikuriya, S.; Kagawa, S. *J. Chem. Soc., Chem. Commun.* **1986**, *16*, 1272.
(40) Da Costa, P.; Moden, B.; Meitzner, G. D.; Lee, D. K.; Iglesia, E. *Phys. Chem. Chem. Phys.* **2002**, *4*, 4590.
(41) *Handbook of Heterogeneous Catalysis*; 2nd ed.; Weinheim: Germany, 2008.
(42) Kokotailo, G. T.; Lawton, S. L.; Olson, D. H.; Meier, W. M. *Nature* **1978**, *272*, 437.
(43) Olson, D. H.; Kokotailo, G. T.; Lawton, S. L.; Meier, W. M. *J. Phys. Chem.* **1981**, *85*, 2238.
(44) Frisch, M. J.; et al. *Gaussian 09*, Revision A.1; Gaussian, Inc.: Wallingford, CT, 2009.
(45) Becke, A. D. *Phys. Rev. A: Gen. Phys.* **1988**, *38*, 3098.
(46) Lee, C.; Yang, W.; Parr, R. G. *Phys. Rev. B: Condens. Matter* **1988**, *37*, 785.
(47) Becke, A. D. *J. Chem. Phys.* **1993**, *98*, 5648.
(48) Mulliken, R. S. *J. Chem. Phys.* **1955**, *23*, 1833.
(49) Mayer, I. *Chem. Phys. Lett.* **1983**, *97*, 270.
(50) Tenderholt, A. L. *QMForge*, v. 2.1. Stanford University: Stanford, CA, 2007; http://qmforge.sourceforge.net.
(51) Hanwell, M. D.; Curtis, D. E.; Lonie, D. C.; Vandermeersch, T.; Zurek, E.; Hutchison, G. R. *J. Cheminform.* **2012**, *4*, 17.
(52) Smeets, P. J.; Sels, B. F.; van Teeffelen, R. M.; Leeman, H.; Hensen, E. J. M.; Schoonheydt, R. A. *J. Catal.* **2008**, *256*, 183.
(53) Johnston, E. M.; Dell'Acqua, S.; Ramos, S.; Pauleta, S. R.; Moura, I.; Solomon, E. I. *J. Am. Chem. Soc.* **2013**, *136*, 614.
(54) Ertem, M. Z.; Cramer, C. J.; Himo, F.; Siegbahn, P. E. *J. Biol. Inorg. Chem.* **2012**, *17*, 687.
(55) Marcus, R. A. *J. Phys. Chem.* **1968**, *72*, 891.